COMPUTATIONAL PLASTICITY

Models, Software and Applications

Edited by:

D. R. J. OWEN

Department of Civil Engineering, University College, Swansea, U.K.

E. HINTON

Department of Civil Engineering, University College, Swansea, U.K.

E. OÑATE

Universitat Politecnica de Catalunya, Spain

Proceedings of the Second International Conference
held in Barcelona, Spain,
18th–22nd September, 1989

PINERIDGE PRESS

Swansea, U.K.

In co-operation with Centro Internacional De Metodos Numericos
En Ingenieria, Barcelona, Spain

MODELING ELASTO-PLASTIC HYSTERETIC BEHAVIORS OF STRUCTURAL STEEL AND APPLICATIONS TO STRUCTURAL MEMBERS

M. Minagawa, T. Nishiwaki and N. Masuda
Musashi Institute of Technology
1-28-1 Tamazutumi, Setagaya-ku, Tokyo 158, JAPAN

SUMMARY

We propose a cyclic plasticity model for predicting quasi-static hysteretic behaviors of steel. The model is based on the "infinite surface model" proposed by Dr. Popov et. al.. It is applied to predictions of tension-compression stress-strain relations of mild steel and high strength steel as well as moment-curvature relations of steel beams. Comparing these relations with experimental results, we confirm the validity of the model proposed here.

1. INTRODUCTION

When elasto-plastic hysteretic behaviors of structures or structural members is predicted with numerical methods such as the finite element method, assumptions introduced in calculation procedures and quality of modeling affect on predicted results. Especially, for local analyses such as local buckling analyses or crack propagation analyses, a proper stress-strain model is needed in order to make predictions accurate.

In order to complement shortcomings of primary models such as the isotropic hardening model [1] and the kinematic hardening model [2,3], a lot of constitutive models had been presented. A model of a field of work hardening moduli, introduced by Mróz [4], corresponds to an extension of the sub-layer model [5] to multi axial stress conditions. In this model, the change in the strain hardening modulus is represented by the concept of movements of multi surfaces defined in the stress field. In this model, a piecewise linear stress-strain relation under proportional loading is assumed [6], and a lot of surfaces should be dealt with in calculating hysteretic behaviors.

The two surface model was presented by Dafalias and

Popov [7,8,9] and Krieg [6] individually in order to prevent the shortcoming. In this model, a bound surface, as a state surface corresponding to an extreme strain state, is introduced in addition to the yield surface. The strain hardening modulus is defined by the configurations and locations of these two surfaces. After the presentation of the two surface model, some amendments are presented [10,11]. But it was pointed out by one of the presenters that "if load reversals take place before any noticeable plastic flow took place in the opposite sense, the updating of the key parameter cannot be done correctly. In this case a progressively greater and greater overshooting of the probable stress path develops -----." [12]. In order to prevent this weak point, Petersson and Popov presented an improved model [12,13]. In this model, infinite intermediate surfaces were introduced between these two surfaces and the complication due to treatment of many surfaces was prevented with an interpolation procedure. It was, however, shown by the authors' investigations that the validity for material with yield plateau and conspicuous strain hardening characteristic was doubtful. Moreover numerical trial-and-error must be done in order to estimate all of material property parameters introduced in the model and then a more rational method for evaluating them should be found. In this paper we propose a modified cyclic plasticity model. As applications of the model, tension-compression stress-strain relations of structural steel and moment-curvature relations of H-shaped steel are predicted and compared with experimental results.

2. PETERSSON-POPOV MODEL [12,13]

Stress-strain relations represented by the Petersson-Popov Model are expressed by means of loading surfaces. Fig.1 explains the concept of this model by combinations of uniaxial stress-strain relations and behaviors of bi-axial multi surfaces for pre-loaded material. In the left figure, a difference between stress-strain relations of the tension path q-a-b-c from a reversed point q and those of the compression path q'-a'-b'-c' is represented by movements and expansions and/or reductions of the surfaces f_0,f_1 and so on.

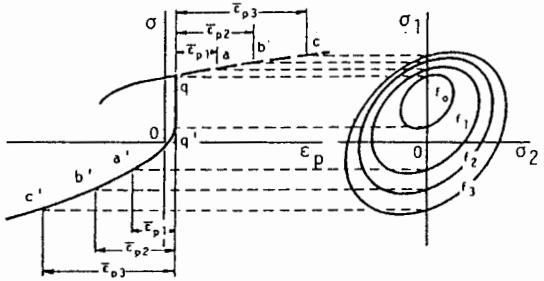

Fig.1 Tension-compression stress-strain relations and corresponding loading surfaces in bi-axial stress space.

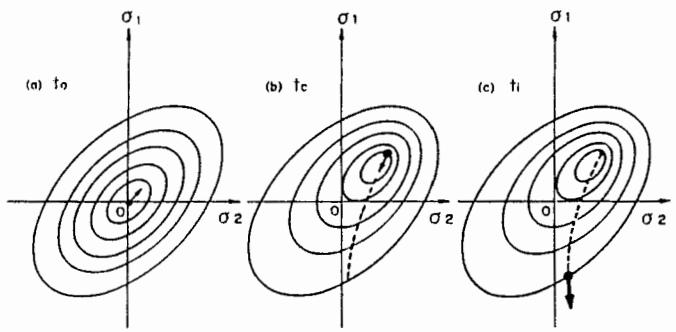

Fig.2 Definitions of times t_o, t_c and t_i in Eq.(2).

Each loading surfaces are defined by a size function and a vector $\{\alpha\}$ indicating those central coordinates [12]. The size function is evaluated as the weighted summation of two functions κ_a and κ_b, which are size functions corresponding to two fundamental loading phases:

$$\kappa = W \kappa_a + (1-W) \kappa_b \qquad (1)$$

where κ_a is the function in the case where no hysteretic effect exists and κ_b is that in the case where the hysteretic effect becomes stationary. These functions are referred to as fundamental size functions in this paper. The weighting function W represents the change in the size function from κ_a to κ_b. The functions κ_a and κ_b are determined from experimental results obtained from a tension test and a tension-compression test and the function W is estimated by means of numerical trial and error.

The following state variables describe the degree of hysteretic effect in this model (see Fig.2):

$$\bar{\varepsilon}_p=\int_{t_o}^{t_c} d\,\bar{\varepsilon}_p, \qquad \bar{\varepsilon}_{pi}=\int_{t_c}^{t_i} d\,\bar{\varepsilon}_p, \qquad d\,\bar{\varepsilon}_p=\sqrt{\frac{2}{3}\,d\,\varepsilon^p_{ij}\,d\,\varepsilon^p_{ij}} \qquad (2)$$

where $\bar{\varepsilon}_p$ is cumulative equivalent plastic strain from the start time (t_o) of loading to the time (t_c) of the last reversal, and ε_{pi} is equivalent plastic strain increment from the time (t_c) to the time (t_i) when the stress-strain relation is to be predicted.

3. PROPOSED CYCLIC PLASTICITY MODEL

The model proposed by the authors is constructed by modifications of the Petersson-Popov Model. Important features of this model are referred to in this section.

3.1 Evaluation of Cumulative Equivalent Plastic Strain

Fig.3 shows two stress-strain curves obtained by

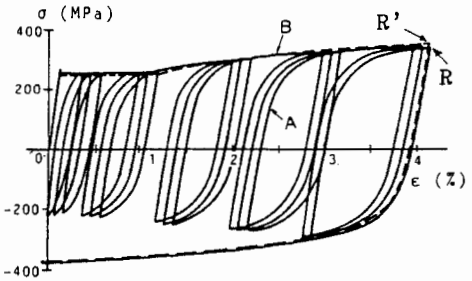

Fig.3 Stress-strain curves with unloading.

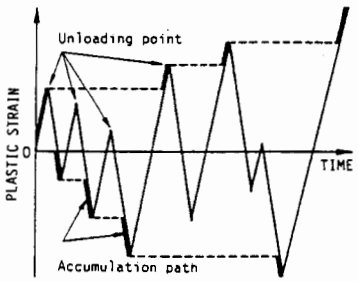

Fig.4 Stress-strain paths for accumulating plastic strain.

experiments. In each test unloading took place at the point R and the point R' respectively. If plastic strain is accumulated over all paths, the cumulative plastic strain at the point R is fairly greater than that at the point R'. But, the stress-strain curve on the path after the point R is much the same as that on the path after the point R'. Therefore we can understand the fact that the plastic strain produced in repetitive loading processes has to be separated in two components: one has an effect on following stress-strain relations and the other does not. Basing on this phenomenon, the cumulative equivalent plastic strain is evaluated under the assumption that the plastic strain beyond the preceding plastic strain amplitude is effective. Thick lines in Fig.4 show the paths on which the plastic strains are to be accumulated in the case of uni-axial loading.

3.2 Choice of Fundamental Size Functions and Institution of Weighting Functions

κ expressing enlargement and reduction of loading surfaces is defined by the following equation:

$$\kappa = W_j \kappa_j + (1-W_j) \kappa_{j+1} \quad ; j=1,N_b \qquad (3)$$

where κ_j and κ_{j+1} are fundamental size functions and W_j is a weighting function expressing the variation in the size of surfaces according to loading histories. The equation means that the variation in the size function in a certain limited range of $\bar{\varepsilon}_p$ can be expressed using the fundamental size functions κ_j and κ_{j+1} defined as size functions at the boundaries determining the range and the weighting function W_j for the range. When the number of boundaries is taken as N_b, an N_b number of weighting functions and an N_b+1 number of fundamental size functions are required.

3.3 Estimation of Material Properties

All of the material properties of the proposed model can be estimated by a combination of a monotonous tension test and several tension-compression tests each including only one

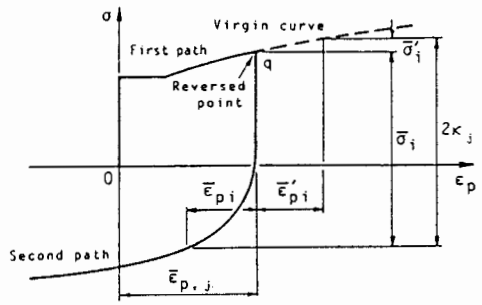

Fig.5 Evaluation of size functions.

reversed point. A procedure evaluating material properties is as follows.

(a) Determination of κ_1.
Virgin stress-plastic strain curve represents κ_1.

(b) Determination of size functions κ_j's.
Size functions κ_j's corresponding to the cumulative plastic strains $\bar{\varepsilon}_{p,j}$'s have to be determined. Using the virgin stress-plastic strain curve and the stress-plastic strain curve obtained by unloading from the point where the cumulative plastic strain reaches $\bar{\varepsilon}_{p,j}$, κ_j is evaluated as the function of $\bar{\varepsilon}_{pi}$. Fig.5 shows how to evaluate κ_j corresponding to the reversed plastic strain $\bar{\varepsilon}_{p,j}$.

(c) Determination of κ_{Nb+1}
κ_j corresponding to the state in which the hysteretic effect becomes stationary is κ_{Nb+1}. The stationary state in hysteretic effect means that no difference is found among each κ_j's. In the case where κ_j's do not converge within the experiments, κ_j for the measured maximum $\bar{\varepsilon}_{p,j}$ is adopted as κ_{Nb+1}.

(d) Determination of W_j
By means of $\kappa_1, \kappa_2, \ldots, \kappa_{Nb+1}$, weighting values for the evaluation of the function κ_j corresponding to the values of $\bar{\varepsilon}_{p,j}$'s are determined by the next equation.

$$W_j = (\kappa - \kappa_{j+1}) / (\kappa_j - \kappa_{j+1}) \qquad (4)$$

Weighting functions are determined by the formula which shows the relation of the weighting values and the corresponding $\bar{\varepsilon}_p$.

4. PREDICTION OF TENSION-COMPRESSION STRESS-STRAIN RELATIONS

4.1 Specimens and Testing Apparatus

Structural steels of SM41A, SM50A and HT70 were used. Table 1 shows the mechanical properties of the steels presented by the steel makers. The configuration of the test specimens used is illustrated in Fig.6. A testing machine with

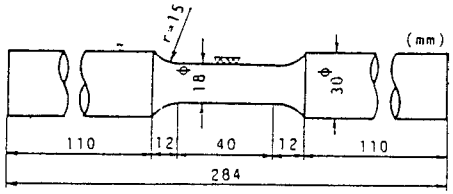

Fig.6
Configuration of test specimens.

	Y.P. (MPa)	T.S. (MPa)	El. (%)
SM41A	284	421	37
SM50A	353	529	28
HT70	622	661	--

Table 1 Mechanical properties.

30 tonf capacity tension-compression actuator was employed and the oil pressure chucking system with 20 tonf capacity was used for setting the specimens. The load was detected by a load-cell attached to the testing machine and the strain was detected by strain gauges. The loading is controlled by the strain at the central section of the test specimens with the strain rate of 0.0001mm/mm/sec.

4.2 Numerical Calculation Method

Elasto-plastic finite element analyses were carried out for round-bar steel specimens subjected to tension-compression repetitive loading under strain control [14,15]. Assumptions introduced in the analyses are as follows;

(1)constant strain triangular finite elements were used,
(2)initial yielding complies with von Mises yield criterion,
(3)yielding was judged with the r-min method [16],
(4)incremental method was used as a nonlinear calculation procedure.

4.3 Comparisons of Experimental and Calculated Results

In order to estimate the size function κ in strain hardening region of two types of steel of SM41A and HT70, three fundamental size functions and two weighting functions shown by Fig.7 and Fig.8 were determined. The fundamental size functions κ_1 and κ_2 correspond to κ_a and κ_b of the

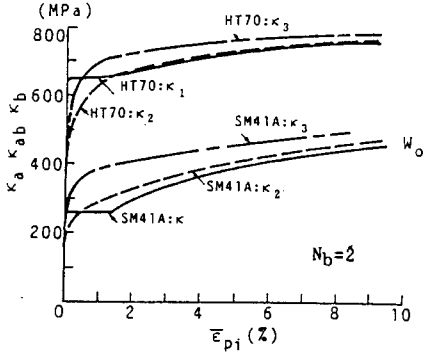

Fig.7 Fundamental size functions of SM41A and HT70.

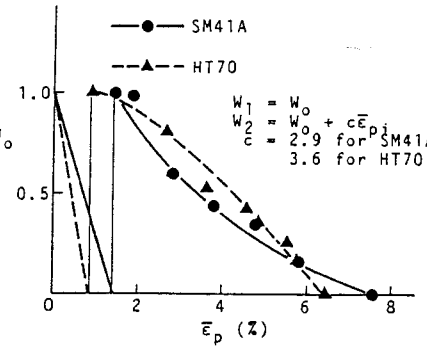

Fig.8 Weighting functions of SM41A and HT70.

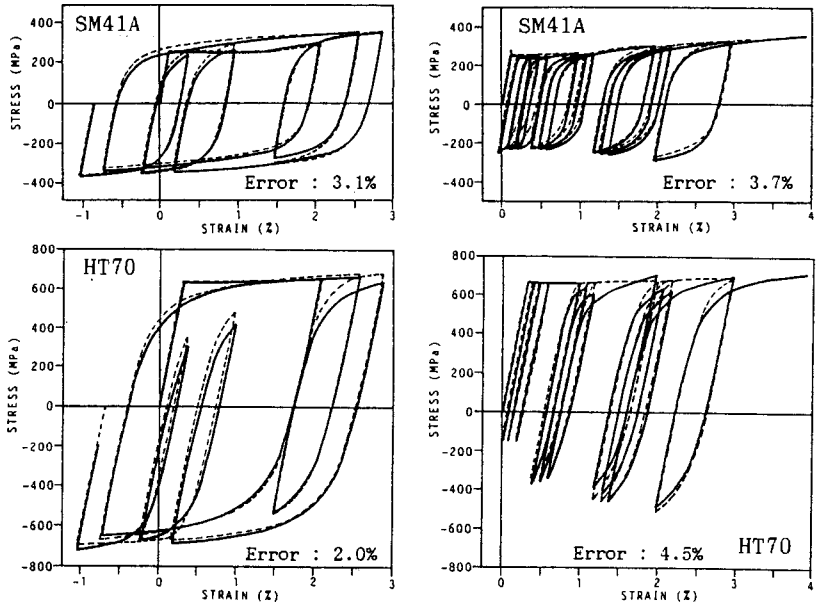

Fig.9 Comparisons of stress-strain relations; the case of strain hardening region.

Petersson-Popov Model, while κ_2 is the function of materials with loading history corresponding to a start point of the strain hardening. One of the weighting function W_1 is assumed to decrease lineary and the other was measured from experimental results. Fig.9 shows stress-strain relations predicted by the proposed model and those gained by the corresponding experiments.

For prediction of stress-strain relations in plastic flow region of SM50A steel, five fundamental size functions and four linear weighting functions were employed. Fig.10 shows fundamental size functions measured. In addition to three functions used in predicting stress-strain relations in the strain hardening region, two more functions were measured and directly used as additional fundamental size functions.

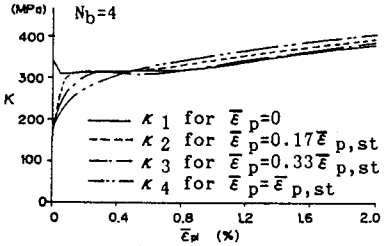

Fig.10
Fundamental size functions of SM50A in plastic flow region.

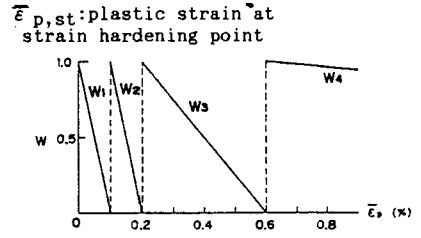

Fig.11
Weighting functions assumed for SM50A.

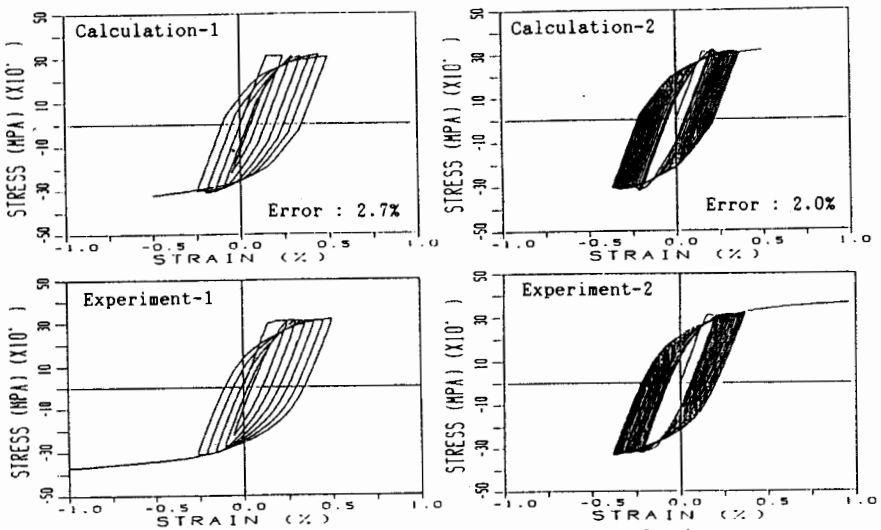

Fig.12 Comparisons of stress-strain relations; the case of plastic flow region.

Therefore, all of the weighting functions were defined as linear functions as shown in Fig.11. Fig.12 shows stress-strain relations and those relations obtained by experiments.

The error measure shown in Fig.9 and Fig.12 is defined as the following equation:

$$\int_{\text{all paths}} |\sigma_{i,\text{cal.}} - \sigma_{i,\text{exp.}}| \, d\varepsilon_i \Big/ \int_{\text{all paths}} |\sigma_{i,\text{exp.}}| \, d\varepsilon_i \times 100 \ (\%) \qquad (5)$$

In spite of the use of material properties determined from fundamental measurements only for some specimens, the stress-strain relations predicted coincide considerably with the measured stress-strain relations.

5. PREDICTION OF MOMENT-CURVATURE RELATIONS OF STEEL BEAMS

5.1 Measurement Method and Material Properties

	Tension test			Chemical composition %					
	Y.P. (Mpa)	T.S. (Mpa)	EL. (%)	C	Si ×100	Mn	P ×1000	S ×1000	Ceq ×100
SS41	312	436	24.5	10	20	60	40	40	21

Table 2 Mechanical properties and chemical compositions

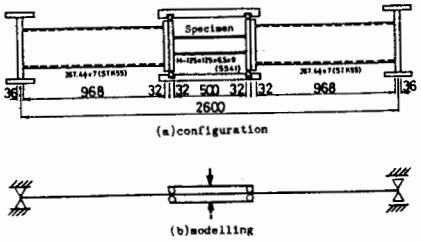

Fig.13 H-shaped steel beam specimen.

	Upper Yield Point σ_{yu}	Lower Yield Point σ_{yl}	Tensile Strength σ_B	Broken Stress σ_b	Young's Modulus ×10^5 E
flange	344	301	440	347	2.10
web	---	402	498	402	2.10

unit : MPa

Table 3 Mechanical properties obtained by tension tests.

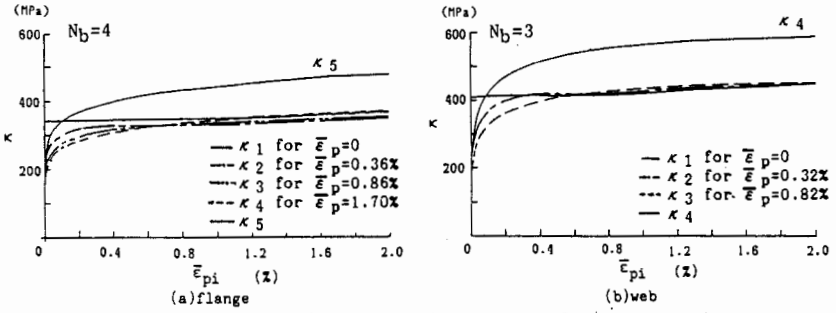

Fig.14 Fundamental size functions for the H-shaped steel.

A specimen consists of a test portion cut out from H-shaped steel of SS41 quality and of two loading arms. The mechanical properties and chemical compositions of the H-shaped steel in the test portion are given in Table 2. The configuration and dimensions of the specimen are shown in Fig.13(a), while the method of loading is shown in Fig.13(b). Loading speed was controlled by mini-computer so that strain rate at the upper and lower flanges would be approximately 0.0001 mm/mm/sec. The curvature of the test portion was calculated with the assumption that cross sections of the beam remain plane.

The mechanical properties measured by tension tests are given in Table 3. To obtain the values for the material properties introduced in the proposed model, a tension-compression tests each including a single unloading were performed besides tension tests.

The fundamental size functions are shown in Fig.14. Since κ_{Nb+1} defined as the fundamental size function when the effects of hysteresis had converged was not measured, the fundamental size function at the time of start of strain hardening enlarged 30 percent in the direction of stress axis was taken to be κ_{Nb+1}, referring to the results of measurements on mild steel shown in Sec.4. All of the size functions measured were adopted as fundamental size functions, and weighting functions were all made to be linear. The residual stresses occurring in the specimens were measured by the hole drilling method and a simple distribution type was assumed.

5.2 Calculation of Moment-Curvature Relations

In case of a frame member having a biaxially symmetrical section, calculations of sectional behaviors can be performed by means of the tangent stiffness method by Chen and Atsuta [17] with some modifications. The hypotheses introduced in numerical calculations are given below.

1) Stress components other than normal stress in the

direction perpendicular to the member cross section are ignored.
2) The configuration of the cross section is invariable.
3) Unstable behavior such as local buckling does not occur.
4) Stress, strain and tangent modulus vary linearly inside each element.
5) Residual stress exists.

In order to evaluate the tangent stiffness, the cross section was divided into finite triangular elements and using the abovementioned hypothesis 4), an integrated value concerning an element was obtained by the values at the three nodal points composing the element.

5.3 Comparisons of Experimental and Calculated Results.

Hysteretic moment-curvature relations were calculated, and compared with those relations obtained by corresponding loading tests. The results are shown in Figs.15. The solid lines of the left figures show the calculated moment-curvature relations and the broken lines the relations obtained from the results of corresponding loading tests, respectively. The stress-strain relation at the top fibers of the upper flange obtained in the numerical calculation are shown in the right figures.

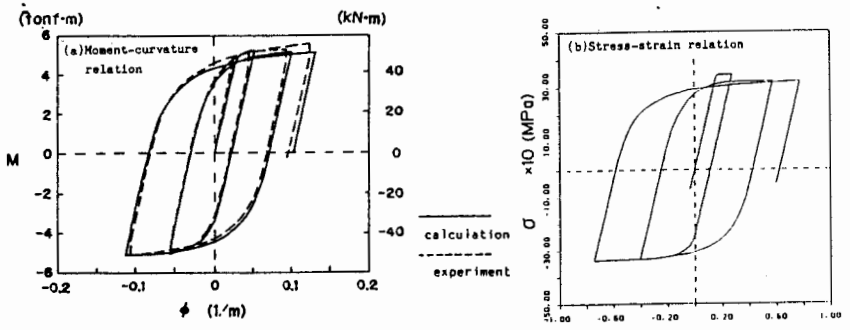

(i) Loading pattern No.1

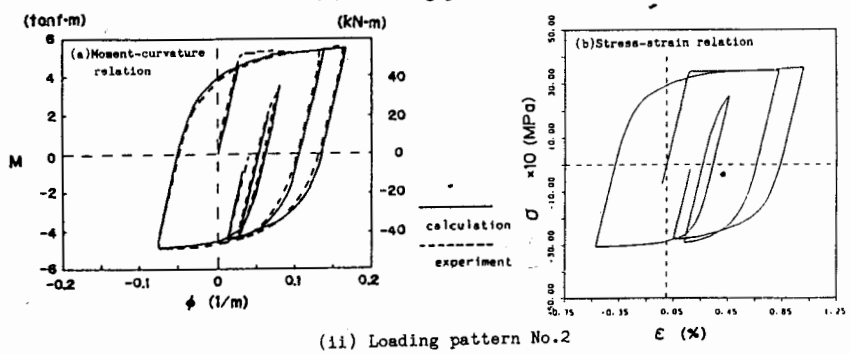

(ii) Loading pattern No.2

Fig.15 Comparisons of moment-curvature relations.

Since the strain to which the material was subjected was about 2 percent at maximum in terms of value of $\bar{\varepsilon}_p$, it can be considered that the effect of having determined κ_{Nb+1} from assumptions based on the measurement results for another type of mild steel has not appeared. As for weighting functions, they were all set linear, and it was found that as a result of having used four or five fundamental surface size functions, serious errors were not brought about in the calculated results. Regarding hysteretic moment-curvature relations, it is thought the errors in the first loading paths have been slightly large mainly because of the scatter in upper yield point values of materials, but it was found concerning subsequent cyclic loading processes that moment-curvature relations obtained from measurements could be predicted with great accuracy.

6. CONCLUDING REMARKS

A cyclic plasticity model proposed here was constructed by refinements of the multi surface plasticity model introduced by Petersson and Popov. We carried out some experiments to measure repetitive stress-strain relations of steel and proposed a model with three significant differences from the Petersson-Popov Model:

(a)Effective value of cumulative equivalent plastic strain is defined as one of state variables.
(b)Additional material property functions are employed. These functions express strain hardening characteristics of materials with certain loading histories.
(c)All of the material property functions can easily be obtained by a combination of a simple tension test and several simple tension-compression tests.

This model was applied to predictions of uniaxial stress-strain relations of mild steel and high strength steel. By comparing the results with those of corresponding experiments, it was confirmed that the accuracy of the stress-strain relations calculated by means of the proposed model was good.

In order to calculate moment-curvature relations of H-shaped beams, the tangent stiffness method was employed by means of cross sectional elements in which stress, strain and tangent modulus vary linearly. The calculated moment-curvature relations were compared with those obtained by experiments and it was shown that the hysteretic moment-curvature relations could be predicted with great accuracy.

References

1. HILL,R.- The Mathematical Theory of Plasticity, Oxford at the Clarendon Press, 1950 (translated into Japanese by WASIZU,K., YAMADA,Y. and KUDO,H., Baihukan, 1954).
2. PRAGER,W. - The theory of plasticity: A survey of recent

achievements, Proc. of the Institute of Mechanical Engineers, 169, p.41, 1955.
3. ZIEGLER,H. - A modification of Prager's hardening rule, Quarterly of Applied Mathematics, 17, p.55, 1959.
4. MRÓZ,M. - An attempt to describe the behaviors of metals under cyclic loading using a more general workhardening model, Acta Mechanica, 7, p.199, 1969.
5. DUWEZ,P. - On the plasticity of crystals, Physical Review, 47, p.494, 1935.
6. KRIEG,R.D.- A practical two surface plasticity theory, Trans. ASME, Jour. Applied Mechanics, 42, p.641, 1975
7. DAFALIAS,Y.F. and POPOV,E.P. - A model of nonlinear hardening materials for complex loadings, Acta Mechanica, 21, p.173, 1975
8. DAFALIAS,Y.F. and POPOV.E.P. - Rate-independent cyclic plasticity in a plastic internal variables formalism, Mechanics Research Communications, 3, p.33, 1976.
9. DAFALIAS,Y.F. and POPOV,E.P. - Plastic internal variables formalism of cyclic plasticity, Journal of Applied Mechanics, Paper No.76-WA/APM-21, American Society of Mechanical Engineers, 43, p.645, December 1976.
10. FUJIMOTO,M., NAKAGOME,T. and YAMADA,Y. - A study based on nonlinear fracture mechanics on fracture of connections in steel structures on cyclic loads, Proc. of the 15th JSSC symposium on matrix methods in engineering, p.161, 1981 (in Japanese).
11. COFIE,N.G. and KRAWINKLER,H. - Uniaxial cyclic stress-strain behaviors of structural steel, Proc. of ASCE, 111, EM9, p.1105, 1985.
12. PETERSSON,H. and POPOV,E.P. - Constitutive relation for generalized loadings, Proc. of ASCE, 103, EM4, p.611, 1977.
13. POPOV,E.P. and PETERSSON,H. - Cyclic metal plasticity ; experiments and theory, Proc. of ASCE, 104, EM4, p.1371, 1978.
14. YAMADA,Y. - Plasticity and Visco-Elasticity, Baihukan, 1970 (in Japanese).
15. YAMADA,Y. and YOKOUCHI,Y. - Programming of Elasto-Plastic Analysis by Finite Element Method - EPIC IV - , Baihukan, 1981 (in Japanese).
16. YAMADA,Y., YOSHIMURA,N. and SAKURAI, T.- Plastic stress-strain matrix and its application for the solution of elastic-plastic problems by the finite element method, International Journal of Mechanical Science, 10, p.343, 1968.
17. CHEN, W.F. and ATSUTA, T.- Theory of Beam-Columns, McGraw-Hill Inc. 1977.